RSC Advances

ROYAL SOCIETY OF CHEMISTRY

www.rsc.org/advances

Journal Name

ARTICLE

Self-assembled nc-Si–QD/a-SiC thin films from Planar ICP-CVD Plasma without H_2-dilution: a combination of wide optical gap, high conductivity and preferred <220> crystallographic orientation, uniquely appropriate for nc-Si solar cells

Received 00th January 20xx,
Accepted 00th January 20xx

DOI: 10.1039/x0xx00000x

www.rsc.org/

Debajyoti Das and Debjit Kar*

Spontaneous miniaturization of self-assembled nc-Si–QDs with preferred <220> crystallographic orientation and a rapid synthesis of superior quality nc-Si–QD/a-SiC thin films of enhanced crystallinity, maintaining a combination of wide optical gap and simultaneous high electrical conductivity, has been attained from (SiH_4 + CH_4)-plasma, without any additional H_2-dilution in inductively coupled plasma CVD. The optical gap widens due to the Si–C bonds in the amorphous network and the increased quantum confinement effect on the miniaturized Si-QDs. CH_4 acts as the dual source of both C and atomic-H. High density of atomic-H available in the planar ICP promotes simultaneously the Si crystallization and its growth along the thermodynamically favored <220> crystallographic orientation, thereby contributing easier electrical transport, particularly at devices in superstrate configuration. After imminent doping those could be efficiently utilized as window layers in third generation all silicon solar cells.

1. Introduction

In photovoltaic technologies, nano-crystalline silicon quantum dots (nc-Si–QDs) embedded in a dielectric matrix is the material of particular interest for its versatile application as window layer in all-Si low-cost third-generation solar cells. In attempting to achieve suitable window layer, there are many reported materials e.g., silicon carbide, silicon nitride and silicon oxide, both in amorphous and nano-crystalline form.[1-9] Owing to the wide optical band gap and high doping efficiency, amorphous hydrogenated silicon carbide (a-SiC:H) has been extensively studied and also successfully employed as window layer for solar cells in *p-i-n* configuration with amorphous silicon (a-Si:H) as absorber *i*-layer. While increasing the optical band gap by higher carbon inclusion in the amorphous network, the electrical conductivity of the a-SiC:H becomes poorer which stands against its efficient utilization in window layers.[1,10,11] In this context, nc-Si–QDs embedded in a-SiC:H could be a better alternative. The widening of the optical gap is provided both by the carbonated amorphous network and the quantum confinement effect arising from the nc-Si QDs which in turn could retain the conductivity from available proportional nanocrystallinity.[12] In addition to maintaining wide optical gap while retaining high conductivity of the doped window layer, the presence of nc-Si component could provide better nucleation path for the growth of crystallites in the intrinsic nc-Si *i*-layer of the nc-Si solar cells which involves better stability due to its lower light induced degradation.[13-16]

Considering its utility in nc-Si solar cells there have been a number of initiatives and various available approaches for the growth of nc-Si QDs e.g., by plasma enhanced CVD (both capacitively and inductively coupled), hotwire CVD, microwave electron cyclotron resonance, helical wave CVD or magnetron sputtering.[17-22] The inclusion of C in the amorphous network leads to the lowering in the degree of crystallinity and this trade-off relation becomes a perpetual hindrance for device application.[11,23] Inductively coupled plasma CVD with very high density of plasma species, low plasma sheath potentials and excellent uniformity of the plasma parameters in the radial and axial directions can provide high density of atomic hydrogen over the growing film surface which could be instrumental in strategic promotion of crystallization in the silicon network even with the C-inclusion.[6,9,13,24-27]

In this context, we report on the formation of self-assembled nanocrystalline silicon quantum dots in amorphous silicon carbide matrix (nc-Si–QD/a-SiC) with a high deposition rate by inductively coupled plasma CVD from (SiH_4 + CH_4)-plasma without any hydrogen dilution[28], and retaining the crystallinity at a high magnitude even after inclusion of a significant amount of carbon into the network. Extensive studies on the effect of increasing C incorporation on the structural, optical and electrical properties of the nc-Si–QD/a-SiC films have been done. Finally, a possible physical mechanism has been projected on the observed properties

Nano-Science Group, Energy Research Unit,
Indian Association for the Cultivation of Science,
Jadavpur, Kolkata – 700 032, INDIA
E-mail (D. Das): erdd@iacs.res.in ;
Fax: +91(33)24732805

and a comparative study has been discussed on the superiority of nc-Si–QD/a-SiC thin films in the perspective of available data in the contemporary literature.

2. Experimental

Thin films of nanocrystalline silicon quantum dots embedded in amorphous silicon carbide matrix (nc-Si–QD/a-SiC) have been synthesized in a low pressure Inductively Coupled Plasma assisted Chemical Vapor Deposition (ICP-CVD) system. Within the cubic plasma chamber of each side 30 cm the heating element is inserted behind the substrate holder to provide a constant temperature of ~300°C during the film growth. The rf field (13.56 MHz) of 350 W has been feed through a low inductance (0.54 μH) four-antenna flat spiral copper tube coil.[27,29]. The rf antenna is separated from the vacuum region across the quartz window. Films are produced from 2 sccm SiH_4 used as the precursor gas and varying the flow rate of CH_4 from 0–35 sccm, as the source of C in the plasma; both being introduced through two separate circular gas rings placed sequentially between the substrate holder and the quartz plate. Samples were deposited on Corning® Eagle2000™ glasses, p-type (100) single crystal silicon wafers and carbon coated Cu microscope grids supplied by Pacific Grid-Tech, USA, for various structural, optical and electrical measurements.

The Dektak 6M profilometer has been used to measure the thickness of the films. The X-ray diffractometry was performed by Cu Kα X-ray radiation (λ=1.5418 Å) source and Bragg diffraction set-up (Rich Seifert 3000P). Raman spectrum was obtained at room temperature in a backscattering geometry by Renishaw inVia Raman Microscope with excitation wavelength of 514 nm from air-cooled Ar^+ laser source, maintaining a low power density ~2 mW/cm^2 in order to avoid local heating on the film surface. The various bonding structures between Si, C and H of the films were investigated from the infrared spectroscopy in the range 400–4000 nm by a Perkin Elmer Spectrum100 FTIR spectrometer. Transmission electron microscopy was performed using a JEOL JSM 2010 system operating at 200 kV. The optical density data of the samples were obtained from absorption and reflection measurements in the UV–visible region, using a double beam spectrophotometer (Hitachi 330, Japan). Electrical conductivity of the samples was measured with coplanar Al electrodes deposited by thermal-evaporation at room temperature and the measurement was carried out in vacuum at 5×10^{-6} Torr at room temperature. The conductivity was evaluated from the current measured by a Keithley 6517A electrometer.

3. Results

The nature of variation in the degree of crystallinity of the nc-Si–QD/a-SiC thin films has been investigated by X-ray diffraction studies, as a function of varying flow rate (F) of CH_4 in the SiH_4 plasma. The nc-Si–QD/a-Si thin film prepared at F= 0 sccm demonstrates significant crystallinity by the characteristic diffraction peaks at 2θ ~ 28.3°, 47.1° and 56.6° corresponding to <111>, <220> and <311> planes of crystalline silicon.[30] At the initial inclusion of CH_4 in the plasma with F= 2 sccm although the crystallinity does not change much, gradual but significant variation in the nature of crystallinity has been identified on farther increase in F. The

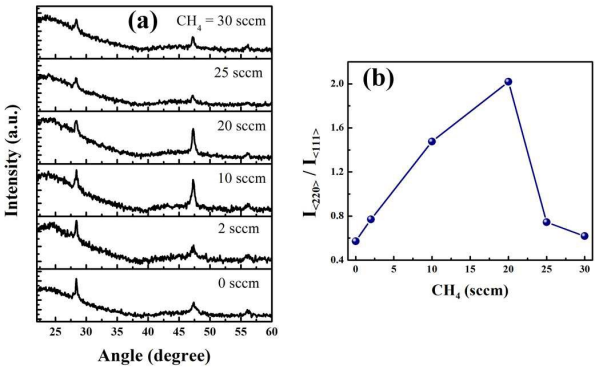

Fig. 1. (a) X-ray diffraction spectra of nc-Si–QD/a-SiC thin films prepared under different flow rates of methane (F). (b) The change in the ratio of <220> to <111> peak intensities, $I_{<220>}/I_{<111>}$, with increasing F.

crystallographic configuration grossly changes from <111> towards <220> preferential orientation, as demonstrated in Fig.1(a). However, for F >20 sccm, the overall crystallinity starts reducing. The nature of changes in the preferred crystallographic orientation with increasing F can be monitored from the variation in relative intensity of <220> to <111> peaks, $I_{<220>}/I_{<111>}$, shown in Fig. 1(b).

The variation in the nature of Si-Si bonding, from crystalline towards amorphous, has been investigated by the normalized Raman spectra shown in Fig. 2(a). At F =0 sccm, the spectrum shows an asymmetric sharp peak at ~516 cm^{-1} corresponding to the predominant crystalline silicon phase, along with its elongated tail towards lower wavenumber as the signature of only a small fraction of accompanying amorphous component in the network. Highly crystalline nature of the pristine silicon thin films is the characteristic of ICP-CVD operating at optimum parametric conditions.[27,29] However, interesting phenomena appears with the incorporation of carbon in the silicon network, by means of increasing F. It has been demonstrated in Fig.2(a) that the nature of the Raman spectra does not change significantly for a systematic increase in CH_4 flow within the plasma up to F ≤25 sccm. However on further increase at F >25 sccm, a drastic change in the nature of the spectra with broad Gaussian peak at ~ 480 cm^{-1} identifies a rapid growth in the amorphous component that turns to the formation of an amorphous dominated silicon network at F =35 sccm.

The degree of crystallinity of the films has been quantitatively characterized by deconvoluting each spectrum into three independent satellite components using a routine least-square fit, after background subtraction. The corresponding three peaks are assigned to: (i) the Lorentzian peak of nano-crystalline silicon (nc-Si) at ~516 cm^{-1}, (ii) an intermediate Gaussian peak at 500–510 cm^{-1} due to ultra-nanocrystalline silicon (unc-Si) or grain-boundary region, and (iii) lastly, a broad Gaussian peak of amorphous silicon (a-Si) at lower Raman shift of 480 cm^{-1}. [31-34] A representative deconvolution of peaks has been shown in Fig. 2(b) and from the integrated area of the deconvoluted components the crystalline volume fraction (F_c) has been estimated, considering the unc-Si component as the part and portion of crystallinity.[13]

Journal Name

ARTICLE

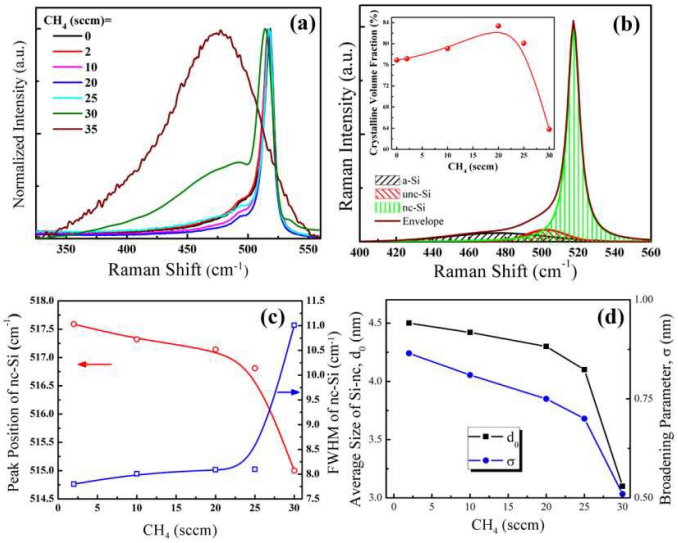

Fig. 2. (a) The normalized Raman spectra of the nc-Si–QD/a-SiC thin films prepared under different flow rates of CH_4 (F). (b) Deconvolution of the Raman spectrum into three satellite components for films prepared at F = 20 sccm. Inset shows the variation in the crystalline volume fraction with increasing F. (c) The shifting of the peak position and widening of the peak width of nc-Si satellite peak with the change in F. (d) The reduction in the average size of the Si-nc and broadening parameter of size distribution with the increase in F.

The remarkable result shown in the inset of Fig. 2(b) demonstrates a systematic enhancement in the crystalline volume fraction (X_C) in the network from ~76.9 to 83.4% for increasing F from 0 to 20 sccm, beyond which X_C starts reducing, followed by a drastic deterioration to 63.8% at F =30 sccm. The results indicate the realization of C-induced promotion of crystallization of Si-network effective for a limited amount of C incorporation under optimized parametric conditions with ICP-CVD.

The systematic peak shift of the nc-Si components towards lower wavenumber along with maintaining the virtually similar narrow line-width realized with increasing F up to 20 sccm, as shown in Fig. 2(c), might be the result of the variations in phonon confinement effect and hence suggest regular reduction in the size of the quantum dots (Si-QD).[30] For crystalline silicon (c-Si), the momentum conservation law restricts the excited phonons at the centre of Brillouin zone in contributing to the first order Raman scattering process. However, with the reduction in size of the crystalline silicon quantum dots, the quantum effect arises in the scattering process. With non-validation of momentum conservation law in the Si-QD, the phonons are dispersed over the Brillouin zone and start contributing in Raman spectra due to spatial confinement of phonons within the Si-QDs by the presence of structural defects at nano-crystalline boundaries. Strong confinement effect occurs when the radius of the Si-ncs approaches the Bohr's radius of silicon (~5 nm) and reduces further.

Accordingly, Raman spectra for the nc-Si peaks have been simulated considering the phonon confinement effect of Si-QDs along with its Gaussian size distribution. To depict the phonon confinement effect in the Raman spectra, a sine wave has been taken as the confinement function which disappears outside the Si-QD boundary and the phonon dispersion curve has been taken as proposed by Paillard.[35] The expression for the first order Raman spectrum is given below –

$$I(\omega,d) \approx \int_0^{0.5} \frac{Sin^2[(qd/a)\pi]dq}{[1-(qd/a)^2]^2[\varpi(q)-\omega]^2+(\Gamma/2)^2} \quad \ldots\ldots(1)$$

where, a is the lattice parameter (0.543 nm), Γ is the natural line-width of bulk crystalline silicon peak which has been taken as 6 cm^{-1} considering the broadening factor arising due to the optical instruments into account. The $\varpi(q)$ is the phonon dispersion relation given by –

$$\varpi(q) = \sqrt{(520)^2 - \frac{121600\times q^2}{q+0.53}} \quad \ldots\ldots(2)$$

The above equations are appropriate for silicon nano-crystals with uniform size (d). However, in reality the Si-QD must have a separate size distribution in each sample. Accordingly, the final expression for the Raman spectrum can be written as –

$$I(\omega) \propto \int f(d)I(\omega,d) \quad \ldots\ldots(3)$$

where, $f(d)$ has been taken in the Gaussian size-distribution as –

$$f(d) = \left(1/\sigma\sqrt{2\pi} \right) \exp\left(-\frac{(d-d_0)^2}{2\sigma^2} \right) \quad \ldots\ldots(4)$$

Here, d_0 is average grain size of Si-QD (apex of the Gaussian distribution) and σ is the size distribution parameter.[23] Fig. 2(d) represents the variation of the average Si-QD size (d_0) and the corresponding size-distribution parameter (σ), as estimated from the above simulation of the Raman spectra, with the flow rate of CH_4 (F). The average size d_0 has been found to reduce from 4.5 to 4.1 nm as F changes from 2 to 25 sccm beyond which a significantly low dimensional nc-Si–QD of size ~3.1 nm has been attained at F =30 sccm. The size-distribution parameter decreases monotonically from 0.87 to 0.51 nm for the increase in F from 0 to 30 sccm.

Systematic variation of crystallization in the nc-Si–QD/a-SiC films with the introduction of CH_4 in the plasma has been studied by transmission electron microscopy (TEM). Fig. 3(a-i) represents the TEM micrograph of the pristine crystalline Si-network prepared at F =0 sccm, where the crystalline Si-QDs, visible as deep dark spots, are randomly dispersed over a relatively bright and homogeneous a-Si network.[36,37] The selected area electron diffraction (SAED) pattern of the films at the inset of Fig. 3(a-i) shows bright diffraction rings, which are identified as the <111>, <220> and <311> planes of crystalline silicon. The presence of such planes has also been previously confirmed by the X-ray diffraction analysis. The high resolution TEM picture in Fig.3 (a-ii) clearly depicts the lattice planes of the crystalline Si-QDs with distinct edges within the amorphous network.

In Fig.3 (b-i), the basic difference in the TEM picture for F =20 sccm, is the better contrast between the crystallites visible with relatively sharp edges. This might be due to the incorporation of C in the amorphous matrix and the Si-QDs have better contrast with the carbonated amorphous network due to larger difference in the density between the crystalline (nc-Si) and amorphous (a-SiC) components. The corresponding SAED picture (inset of Fig. 3 (b-i)) shows three prominent diffraction rings and spotted features, which identify higher degree of crystallinity. In plain-view HR-TEM micrograph the <220> crystal planes are relatively difficult to be visible because of their specific geometrical projection on two-dimensional plane, compared to its <111> counterpart. Spontaneous detection of the (220) lattice planes of c-Si on arbitrarily chosen area of the sample, as shown in Fig. 3(b-ii), establishes the presence of a significant number of <220> oriented nc-Si–QDs within the a-SiC matrix prepared at F =20 sccm. It is to be noted that for this nc-Si–QD/a-SiC film a significantly high magnitude of $I_{<220>}/I_{<111>} \geq 2$ has been demonstrated by the XRD studies, identifying <220> preferential orientation. For further increase in F, however, the major change arises in the reduced size of the Si-QDs and their gradual amorphization.

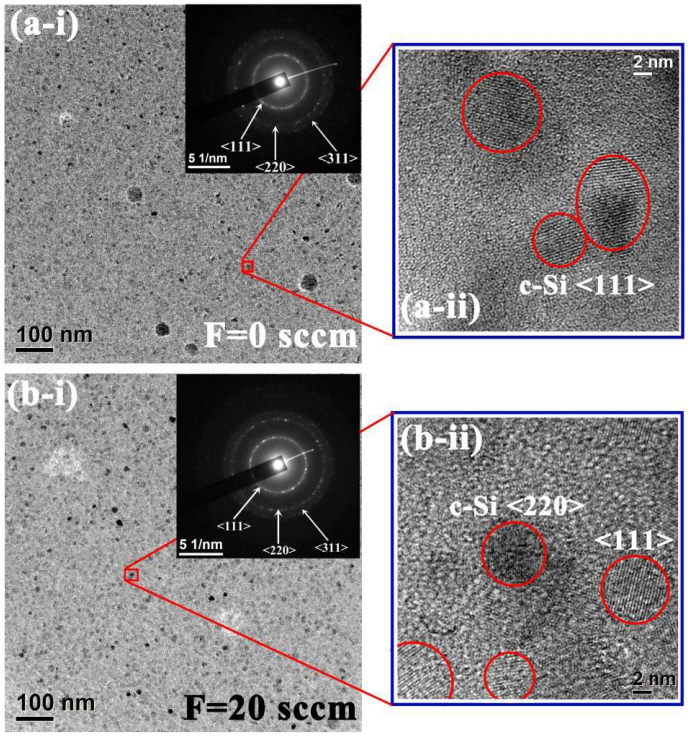

Fig. 3. (a-i) and (b-i) The TEM micrographs of the nc-Si–QD/a-SiC films prepared at different flow rate of CH_4 (F), as noted in individual figures. Insets show the SAED pattern of the corresponding degree of crystallinity. (a-ii) and (b-ii) HRTEM images of arbitrarily selected Si-nano-crystals of <111> and <220> crystallographic orientations of crystalline silicon.

Journal Name

ARTICLE

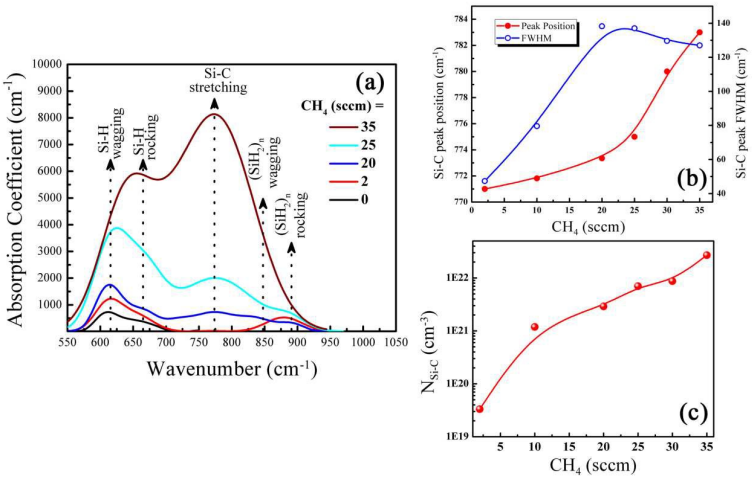

Fig. 4. (a) The infra red absorption spectra for the films prepared at increasing F, identifying different bonding configuration between Si, C and H. (b) The variation in the peak position and FWHM of the Si-C peak. (c) The enhancement in the estimated Si-C bond density at higher flow rate of CH_4.

The bonding configurations between Si, C and H has been investigated by the infrared spectroscopy, performed on the films deposited on Si-wafers. The spectra have been corrected for the substrate absorption, and normalized by the film thickness. The absorption spectra of the films have major peaks mainly in two spectral ranges around ~550-950 cm^{-1} and 1900-2100 cm^{-1}; the first range corresponds to the Si-H wagging and Si-C stretching modes absorptions while the second range arises due to the stretching mode vibration of silicon hydrides (not shown here).Fig. 4(a) shows the absorption spectra for films prepared at various flow rates of CH_4 in the lower wavenumber range. The pristine silicon thin film with F =0 sccm shows a dominant peak at ~620 cm^{-1} due to the wagging mode of Si-H vibration while the extended tail towards higher wavenumber at ~670 cm^{-1} corresponds to the Si-H rocking mode. With the introductory inclusion of CH_4 in the plasma at F =2 sccm, the intensity of the wagging mode has been enhanced with the appearance of a separate peak at ~880 cm^{-1}, which is due to the wagging and rocking modes of $(SiH_2)_n$.[38,39] For F >2 sccm, the additional peak that starts prominently appearing in the spectra at ~780 cm^{-1} corresponds to the Si-C stretching mode absorption. All the absorption peaks rapidly increase in intensity at higher flow rates of CH_4, F >20 sccm.

Each spectrum has been deconvoluted into five components as identified in Fig. 4(a) and the corresponding data for the most prominent Si-C stretching band at ~780 cm^{-1} has been plotted in Fig. 4(b). The peak position has been observed to shift substantially towards higher wave numbers along with rapid widening in the corresponding FWHM for increasing F till ≤20 sccm, as a consequence of larger number of C-atoms being systematically attached to the Si-network and changing the overall structural ordering of the amorphous matrix. For F >20 sccm, however, a significantly fast shift in the peak position identifies larger number of C-atoms being attached to single Si-atom. Increasing number of C-atom consequences in elevated polarity in the Si-C bond, resulting in the shift of peak position.[40] The virtual saturation of the corresponding FWHM represent a narrow spreading of bond lengths and low distortion of the bond angles, perhaps characterizing the formation of small fraction of SiC crystalline state.[41]

The bond density of Si-C (N_{Si-C}) has been estimated from the integrated area under the Si-C stretching mode peak using the following relation:

$$N_{Si-C} = A \int_{Si-C} \frac{\alpha(\varpi)}{\varpi} d\varpi \qquad \ldots\ldots(5)$$

where, $\alpha(\varpi)$ is the absorption coefficient and ϖ is the wave number and $A = 2.13 \times 10^{19}$ cm^{-2} for the corresponding mode of vibration.[42] At the initial introduction of CH_4 in the plasma the Si-C bond density, N_{Si-C}, increases very rapidly. However, for F >10 sccm the rate of C inclusion stabilizes and a gradual enhancement in the Si-C bond density has been identified, as shown in Fig. 4(c). About three orders of magnitude increase in Si-C bond density has been estimated over the entire span of increasing F from 2 to 35 sccm. However, the absence of any C-H stretching mode absorption band at around 2900 cm^{-1} in the IR spectra indicates about an overall below stoichiometric silicon–carbon network in the films under investigation.[43]

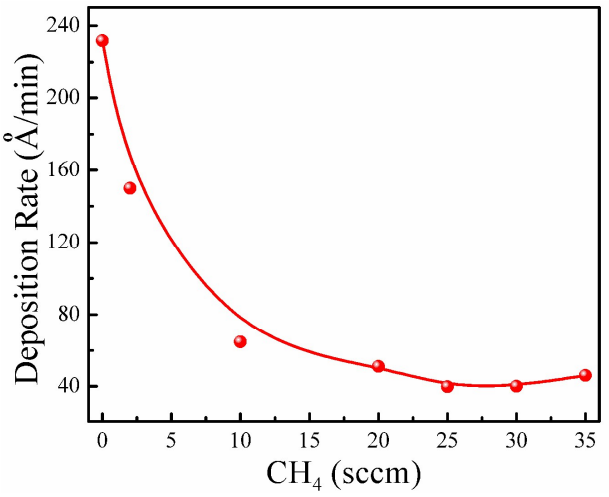

Fig. 5. The decay in the deposition rate with the enhancement of methane flow rate in the plasma.

The pristine silicon thin films have been obtained at a high deposition rate ~230 Å/min which is significantly high compared to similar films grown from commonly used capacitively coupled plasma CVD with hydrogen dilution, in which it is typically 3 Å/min.[44] With the introduction of CH_4 in the plasma the deposition rate of the nc-Si–QD/a-SiC thin films reduces abruptly to ~65 Å/min at F =10 sccm, as shown in Fig. 5. For further addition of CH_4 the deposition rate, however, virtually attains a sallow saturation. The reduced deposition rate at increased CH_4 dilution arises due to the reduced SiH_n radical density in the plasma. In addition, methane molecules have the dissociation energy (~413.0 kJ mol^{-1}) higher than that of the silane molecules (~299.2 kJ mol^{-1}) and the carbon based radicals have a much lower sticking coefficient compared to the silicon-based radicals. These two factors act in accord and eventually lead to the lower deposition rate of the films. In addition, the reduced fraction of SiH_n radicals in the plasma at higher flow rate of CH_4 encounters with rather higher number of atomic H decomposed from increased total flow of feedstock (SiH_4 + CH_4), which further influences in reducing the growth rate of the material due to increased atomic H etching.[45]

The optical band gaps of the nc-Si–QD/a-SiC thin films have been estimated from the standard Tauc's plot of the absorption spectra in the UV-visible region following:

$$\sqrt{\alpha E} \propto (E - E_g) \qquad \ldots\ldots(6)$$

where α is the absorption coefficient and E is the photon energy. The optical gap (E_g) of the pristine crystalline silicon film prepared at F =0 sccm has been estimated as ~1.81 eV which undergoes a sharp increase to 1.86 eV at the initial introduction of CH_4 in the plasma with F = 2 sccm, as shown in Fig. 6. With the further increase of F up to 20 sccm, E_g increases gradually at a lower slope and attains a magnitude of ~1.89 eV. For F >20 sccm, a significantly different mode of optical band gap enhancement has been depicted in Fig. 6, at F =35 sccm largely amorphous dominated silicon carbon alloy film attains a wide optical gap, E_g =2.03 eV.

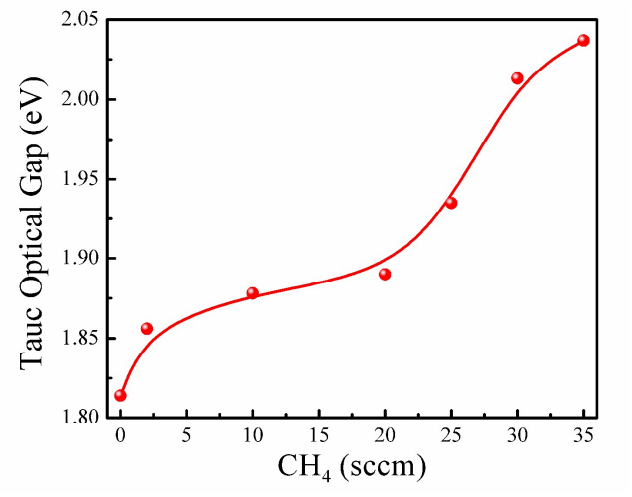

Fig. 6. The widening of the Tauc optical gap at higher flow rate of CH_4.

The electrical conductivity of the films has been studied in co-planer configuration with aluminium electrodes. The dc dark conductivity, σ_d, has been plotted in Fig. 7 with the CH_4 flow rate as a parameter. The pristine crystalline silicon thin films possess a high σ_d ~8.2×10^{-9} S cm^{-1}. With the incorporation of CH_4 in the plasma, the conductivity has been improved significantly to 2.01×10^{-4} S cm^{-1} at F =20 sccm. However, for higher F, the σ_d starts reducing very fast and attains a very low magnitude of 8.47×10^{-11} S cm^{-1} at F =35 sccm, where the film is dominantly amorphous in nature.

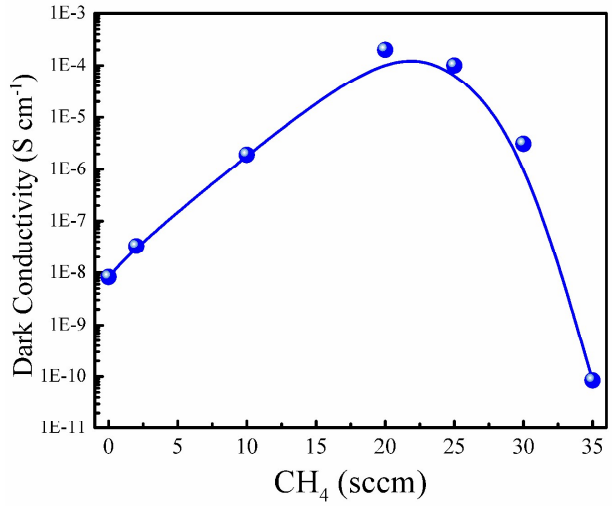

Fig. 7. The variation in the dark electrical conductivity showing very high magnitude of ~10^{-4} S cm^{-1} at F=20 sccm.

4. Discussions

Let us now interpret the experimental results on the structural, optical and electrical properties of the nc-Si–QD/a-SiC films, as the effect of systematic inclusion of C into the highly crystalline pristine silicon network, obtained by means of introducing CH_4 in the SiH_4 plasma without any hydrogen dilution. It has been observed that the way most of the properties depend on the flow rate of CH_4 (F) have

two different regions. For 0 ≤ F (sccm) ≤ 20, the deposition rate reduces sharply, the carbon incorporation into the amorphous matrix is low, the overall crystallinity has been improved with minor decrease in the average size of the Si-QDs having preferred growth orientation along <220> lattice planes of silicon, finite widening in the optical band gap, although a significant improvement in the dark electrical conductivity by about four orders of magnitude. Further increase in F beyond 20 sccm consequences a sallow saturation of the deposition rate, higher Si-C bond density, sharp reduction in crystallinity with significant miniaturization of Si-QDs having grossly reduced intensity of <220> c-Si planes, a significant enhancement in the optical band gap along with a sharp lowering of the electrical conductivity by several orders of magnitude. At very high magnitude of F (=35 sccm), however, the film becomes structurally amorphous dominated.

In a multi-phase network where nc-Si–QDs are dispersed in the a-SiC matrix, the optical gap, E_g, is governed by the contributions from both the phases. Accordingly, E_g might have dominant contributions from two parameters: i) average size of Si QD along with the overall crystallinity, and ii) Si-C bond concentration in the amorphous matrix. The optical band gap, E_g, of the mixed phase material can be empirically presented as: $E_g = E_{Si\text{-}QD} + E_{a\text{-}SiC}$, where $E_{Si\text{-}QD}$ arises from the quantum confinement effect of the Si-QDs and is inversely proportional to the square of their radius, while the $E_{a\text{-}SiC}$ depends on Si-C bond density and the bonded H-content in the network.[13,41,46] During the enhancement of CH_4 flow rate in the range F ≤20 sccm, replacement of the weaker Si-Si bonds by stronger Si-C bonds help increasing the $E_{a\text{-}SiC}$ component,[44] in addition, minor reduction in the size of Si-QDs leads to the enhanced quantum confinement effects and hence a subsequent widening of the optical gap. In the higher range of CH_4 flow, F ≥25 sccm, in addition to a larger amount of C inclusion into the Si-network and its subsequent influences, a reasonably large reduction in the size of Si-QDs (from 4.1 to 3.1 nm) within Bohr-radius zone induces significantly in the band gap widening, resulting in a notable overall enhancement in the E_g of the nc-Si–QD/a-SiC network, as demonstrated in Fig. 6.

It has been observed with interest that during increasing C incorporation into the Si network in the form of Si-C bonds and the subsequent widening of the optical gap of the nc-Si–QD/a-SiC network, corresponding to increasing F in the range 0 ≤ F (sccm) ≤ 20, the dark electrical conductivity increases by four orders of magnitude. From structural and elemental analysis, the nc-Si–QD/a-SiC films can be considered as an array of crystalline Si-QDs embedded in insulating amorphous Si:H and/or SiC matrix. In such multi-phase thin film structures, the prevalent transport mechanism is based on percolation of carriers (which are thermally activated to conduction band) between the crystalline grains through the amorphous tissue.[47] There are two competing factors in controlling the electrical transport properties in the films – the crystalline part with higher mobility promoting the transport properties and the insulating barrier layer of amorphous part, controlled by the Si-C bond density, hindering the transport of charge carriers. At F =0 sccm, the film is highly crystalline (X_C ~76.9 %) with grains of average size ~4.5 nm which provide good conducting-path for the carriers. In the region 0 ≤ F (sccm) ≤ 20, the crystalline volume fraction is increased as well as the size of the Si-QDs reduces. The influence of increasing number density of the crystallites with their reduced size leads over the Si-C bond density in terms of electrical transport by reducing the average inter-QD distance, resulting in the overall improvement in the dark electrical conductivity.[29] In addition, the very remarkable feature of the Si-QDs are their dominent growth along the thermodynamically most favoured <220> crystallographic orientation, compared to the regular growth along <111> direction and that reaches a magnitude as high as $I_{<220>}/I_{<111>} \geq 2$. The closer lattice planes of <220> orientation provides superior conduction path to the charge carriers compared to the <111> planes. Altogether, a significant increase in the electrical conductivity by four orders of magnitude to $\sigma_d \sim 2 \times 10^{-4}$ S cm^{-1} has been realized. For F >20 sccm, both the sharply reduced crystallinity and the enhanced Si-C bond density influence uni-directionally on deteriorating the electrical transport, leading to a sharp decay of the dark conductivity. At F = 35 sccm, the films becomes predominantly amorphous in nature with very high density of Si-C bonds which restricts the conductivity at a very low magnitude of 8.47×10^{-11} S-cm^{-1}.

It is noteworthy to observe that the way carbon inclusion have changed the structural, optical and electrical properties of the pristine silicon network is surprisingly unusual compared to the regular reports from available literature, however, significantly useful for device application. In general, the thin films of nano-crystalline silicon quantum dots (nc-Si–QD) embedded in amorphous silicon carbide matrix have been fabricated from the hydrogen diluted (SiH_4 + CH_4)-plasma in a commonly used capacitively coupled plasma CVD. Systematic inclusion of C into the Si-network, in general, introduces deviation from crystallinity and reduction in electrical conductivity, although the optical band gap widens. On the contrary, present experimental results lead to the finite increase in crystallinity with simultaneous significant improvement in electrical conductivity while widening the optical band gap due to limited inclusion of C into the Si-network. In addition, H_2-dilution not being essential in the present experiment with ICP-CVD, the nc-Si–QD/a-SiC films are obtained with a growth rate much higher than the same from conventional capacitively coupled PECVD where a very high degree of H_2-dilution is a prerequisite in promoting crystallization to the Si-network.

In comparison with the conventional capacitively coupled plasma sources, the ICP-CVD operating in the electromagnetic mode have several major advantages e.g., they have: (i) very high densities of the plasma species, in particular, the electron number density ~ 10^{12} cm^{-3} at 10 mTorr, (ii) low plasma sheath potentials (several or tens of volts) near the deposition substrate, which is advantageous for the reduction in ion bombardment on the deposited thin films, (iii) low electron temperatures (a few electron volts) under a broad range of discharge conditions, and (iv) excellent uniformity of the plasma parameters in the radial and axial directions. High density of plasma species, e.g., SiH_n/CH_n (n ≤3) as well as atomic-H contribute both in enhancing growth rate and in promoting crystallization, simultaneously.[20,45,48] The best reported value of the deposition rate for Si-QDs in a-SiC matrix fabricated in ICP-plasma has been attained at an exorbitantly high RF-power at 2000 W which is not compatible for device fabrication.[44] The present work demonstrate

the growth of nc-Si–QD/a-SiC thin films prepared at a low RF power of 350 W and with a reasonably high deposition rate of 24 nm/min which is much higher than the typical deposition rate of 0.3 nm/min for similar films prepared in capacitively coupled RF-PECVD.

It was previously reported that the growth along the thermodynamically preferred <220> planes are formed at elevated temperature and high pressure.[49] Under particular parametric conditions of plasma, near the amorphous to nano-crystalline phase transition region a higher <220> peak intensity can be detected, compared to that for highly crystalline Si. On the contrary, the present investigation identifies the predominant growth of Si-ncs along the <220> planes with intensity $I_{<220>}/I_{<111>} \geq 2$ within a highly crystalline network (~84%), at a low pressure and moderately low temperature. Such dominant crystalline growth along the thermodynamically preferred orientation might be attributed to the inductively coupled plasma with its specific characteristics mentioned above,[27,30] including its associated high density of atomic hydrogen arising from the dissociation of the SiH_4 and CH_4. The highly energetic atomic hydrogen helps promoting the thermodynamically preferred growth by means of chemical annealing on the film growing surface. The <220> oriented growth in Si nano-crystals directly stimulates the performance of solar cells. The charge carriers, whose transport path is normal to the substrate in the nc-Si solar cells in superstrate configuration, observe fewer grain boundaries in (220) oriented grains and thereby, reduced bulk recombination and/or field losses increase the open circuit voltage (V_{OC}) and the Fill Factor (FF).[50]

In view of its effective application as the window layer in all silicon *p-i-n* solar cells in superstrate configuration, the nc-Si–QD/a-SiC films must have wide optical gap with very high electrical conductivity. However, generally a trade-off relation holds between these two optical and electrical properties. Present investigation identifies some deviation in this perpetual trade-off relation, the dark conductivity has been improved significantly even with the widening of the optical gap in nc-Si–QD/a-SiC films during incorporation of a small amount C in a stringent parametric condition with ICP-CVD. In this context a comparative study has been made on the optical gap vs. dark conductivity relation among various undoped a-/μc-/nc-silicon–carbon-alloy thin films available in the literature. As shown in Fig. 8, the works by Yunazet. *et. al.*, Demichelis *et. al.* and Li *et. al.* have shown very poor conductivity for amorphous silicon carbide films compared to the present data at equivalent band gaps.[51-53] In the report by Lee *et. al.*, the nc-Si/a-SiC thin films showed very high optical gap with conductivity comparatively higher than the a-SiC films.[12] However, the band gap was reported in terms of E_{04} which is supposed to be higher than the Tauc's optical gap discussed here. Among the referred sets of data, only those from Coscia et. al. and the present report have closer conductivity at around E_g ~1.90 eV, yet the conductivity for the present set of samples is superior for the region of band gap, $1.9 \leq E_g(eV) \leq 2.04$.[10] However, there are several reports which demonstrate the development of μc-SiC thin films having very high electrical conductivity even at a wider optical band gap.[54,55] Such thin films have been utilized by Hamakawa *et. al.* as the

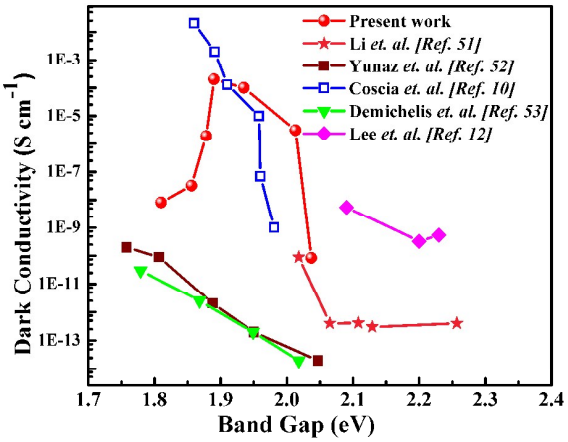

Fig. 8. A comparative study on the dark electrical conductivity at room temperature vs. band gap profile, among various undoped amorphous or micro/nano-crystalline silicon–carbon alloy thin films available in the literature.

window layer in the hetero-junction solar cells with a-Si:H *i*-layer in the glass/TCO/*p*-μc-SiC/*i*-a-Si:H/*n*-μc-Si/Ag configuration.[56] However, in view of developing nc-Si solar cells, the spontaneous subsequent growth of the nc-Si *i*-layer on the μc-SiC thin films will be obstructed due to the lattice mismatch between crystalline SiC and Si. In order to surpass such obstacle, another layer needs to be deposited in between those two layer,[57] which leads to obvious technological inconvenience. On the contrary, the present nc-Si–QD/a-SiC thin films, developed at a reasonably high growth rate from spontaneous (SiH_4+CH_4)-plasma processing without H_2-dilution by ICP-CVD, with its wide optical band gap and high electrical conductivity, possess adequate prospect for its future use in the window layer of nc-Si solar cells, in particular.

5. Conclusions

The present manuscript deals with the synthesis of nanocrystalline Si quantum dots embedded in an amorphous SiC matrix (nc-Si–QD/a-SiC) with a high deposition rate from the gas mixture of silane and methane without any additional hydrogen dilution, using spontaneous plasma processing by inductively coupled plasma CVD. The CH_4 flow in the plasma acts as dual source of both carbon and atomic hydrogen. During limited increase in CH_4-dilution in the plasma, increasing C-incorporation into the amorphous matrix surrounding the crystalline silicon quantum dots (Si-QDs) continuously miniaturizes the size of the Si-QDs. However, simultaneous increase in atomic H extracted from CH_4 plays over the effect of C inclusion in introducing newer nucleation sites and thereby enhancing the overall crystallinity. In addition, atomic H at higher density promotes the Si crystallization along thermodynamically favourable <220> crystallographic orientation, compared to <111>, by means of chemical annealing. The optical gap widens due to the larger number of Si–C bonds in the amorphous network and the increased quantum confinement effect on the miniaturized Si-QDs at increasing CH_4 dilution to the SiH_4 plasma. The presence of Si-QDs with preferred <220> crystallographic orientation available in the hetero-structure at the

higher crystalline volume fraction contribute simultaneously in maintaining high electrical conductivity in the nc-Si solar cells in superstrate configuration. Altogether, the nc-Si–QD/a-SiC films demonstrate a significantly high electrical conductivity ~10^{-4} S cm^{-1} at an wide optical band gap ~1.90 eV, with which the conductivity for the present set of samples, in the region of band gap $1.9 \leq E_g$ (eV) ≤ 2.04, has been found to be superior to the data available in the literature.

Finally, the present work enables the spontaneous minaturization of self-assembled nc-Si–QDs with preferred <220> crystallographic orientation and a rapid growth of superior quality nc-Si–QD/a-SiC thin films of enhanced crystallinity, maintaining a combination of wide optical gap and simultaneous high electrical conductivity; after imminent doping those could be efficiently utilized as window layers in third generation all silicon solar cells.

Acknowledgement:

The work has been done under nano-silicon projects funded by the Department of Science and Technology (Nano-Mission Program) and the Council of Scientific and Industrial Research, Government of India. The HR-TEM studies have been performed using facilities of the Unit on Nano-Science at IACS.

References:

[1] Y. Tawada, M. Kondo, H. Okamoto and Y. Hamakawa. *Sol. Energ. Mater.* 1982, **6**, 299-315.

[2] Y. Matsumoto, F. Meléndez and R. Asomoza. *Sol. Energ. Mater. Sol. Cells.* 2001, **66**, 163-170.

[3] D. Das, M. Jana and A.K. Barua. *Sol. Energ. Mater. Sol. Cells*. 2000, **63**, 285-297.

[4] D. Das and A.K. Barua. *Sol. Energy Mat. & Sol. Cells*, 2000, **60**, 167-179.

[5] S.Y. Myong, S.S. Kim and K.S. Lim. *J. Appl. Phys.*, 2004, **95**, 1525-1530.

[6] D. Das and A. Samanta. *Nanotechnology*, 2011, **22**, 055601.

[7] P.D. Veneri, L.V. Mercaldo and I. Usatii. *Appl. Phys. Lett.*, 2010, **97**, 023512.

[8] S. Ogawa, M. Okabe, T. Itoh, N. Yoshida and S. Nonomura. *Thin Solid Films*, 2008, **516**, 758-760.

[9] B. Sain and D. Das. *Phys. Chem. Chem. Phys.*, 2013, **15,** 3881-3888.

[10] U. Coscia, G. Ambrosone, S. Lettieri, P. Maddalena, P. Rava and C. Minarini. *Thin Solid Films*, 2003, **427**, 284-288.

[11] U. Coscia, G. Ambrosone, S. Lettieri, P. Maddalena, V. Rigato, S. Restello, E. Bobeico and M. Tucci. *Sol. Energ. Mater. Sol. Cells*, 2005, **87**, 433-444.

[12] J.E. Lee, S.K. Ahn, J.H. Park, J. Yoo, K.H. Yoon, D. Kim and J. S. Cho. *Prog. Photovoltaics Res. Appl.* (2015) DOI: 10.1002/pip.2605.

[13] D. Kar and D. Das. *J Mater. Chem. A*, 2013, **1**, 14744-14753.

[14] Z. Hu, X. Liao, H. Diao, Y. Cai, S. Zhang, E. Fortunato and R. Martins. *J. Non-Cryst. Solids*, 2006, **352**, 1900-1903.

[15] T. Fujibayashi and M. Kondo. *J. Appl. Phys.*, 2006, **99,** 043703.

[16] K. Adhikary and S. Ray. *J. Non-Cryst. Solids*, 2007, **353**, 2289-2294.

[17] D. Das and M. Jana. *Sol. Energ. Mater. Sol. Cells*, 2004, **81**, 169-181.

[18] H. Jia, H. Shirai and M. Kondo. *J. Appl. Phys.*, 2007, **101**, 114912.

[19] D. Raha and D. Das. *Sol. Energ. Mater. Sol. Cells*, 2011, **95**, 3181-3188.

[20] M.A.L.a.A.J. Lichtenberg, Principles of PlasmaDischarges and Materials Processing, Wiley Interscience, New York, (1994).

[21] Y. Wei, L. Wanbing, H. Li and F. Guangsheng. *J. Phys. D: Appl. Phys.*, 2004, **37**, 3304.

[22] K.N. Ostrikov, S. Xu and M.Y. Yu. *J. Appl. Phys.*, 2000, **88,** 2268-2271.

[23] D. Das and D. Kar. *Phys. Chem. Chem. Phys.*, 2014, **16**, 25421-25431.

[24] H.K. John. *Plasma Sources Science and Technology*, 1996, **5**, 166.

[25] C. Qijin, S. Xu, J.D. Long, Z.H. Ni, A.E. Rider and K. Ostrikov. *J. Phys. D: Appl. Phys.*, 2008, **41**, 055406.

[26] S. Xu, K.N. Ostrikov, Y. Li, E.L. Tsakadze and I.R. Jones. *Phys. Plasmas*, 2001, **8**, 2549-2557.

[27] D. Raha and D. Das. *Appl. Surf. Sci.*, 2013, **276**, 249-257.

[28] C. H. Cheng, Y. H. Lin, J. H. Chang, C. I. Wu and G. R. Lin. *RSC Adv.*, 2012, **4**, 18397.

[29] D. Das and B. Sain. *J. Appl. Phys.*, 2013, **114**, 073708.

[30] B. Sain and D. Das. *Sci. Adv. Mater.*, 2013, **5**, 188-198.

[31] S. Guha, G. Hendershot, D. Peebles, P. Steiner, F. Kozlowski and W. Lang. *Appl. Phys. Lett.*, 1994, **64**, 613-615.

[32] Y.L. He, Y.Y. Wei, G.Z. Zheng, M.B. Yu and M. Liu. *J. Appl. Phys.*, 1997, **82**, 3408-3413.

[33] G.Z. Yue, J.D. Lorentzen, J. Lin, D.X. Han and Q. Wang. *Appl. Phys. Lett.*, 1999, **75**, 492-494.

[34] M. Jana, D. Das and A.K. Barua. *Sol. Energ. Mater. Sol. Cells*, 2002, **74**, 407-413.

[35] V. Paillard, P. Puech, M.A. Laguna, R. Carles, B. Kohn and F. Huisken. *J. Appl. Phys.*, 1999, **86**, 1921-1924.

[36] Q. Cheng, E. Tam, S. Xu and K. Ostrikov. *Nanoscale*, 2010, **2**, 594-600.

[37] D. Das. *Thin Solid Films*, 2005, **476**, 237-245.

[38] G. Lucovsky, J. Yang, S.S. Chao, J.E. Tyler and W. Czubatyj. *Phys. Rev. B*, 1983, **28**, 3225-3233.

[39] A. Samanta and D. Das. *Sol. Energ. Mater. Sol. Cells*, 2009, **93**, 588-596.

[40] U. Coscia, G. Ambrosone and D.K. Basa. *J. Appl. Phys.*, 2008, **103,** 063507.

[41] T. Rajagopalan, X. Wang, B. Lahlouh, C. Ramkumar, P. Dutta and S. Gangopadhyay. *J. Appl. Phys.*, 2003, **94**, 5252-5260.

[42] D.K. Basa and F.W. Smith. *Thin Solid Films*, 1990, **192**, 121-133.

[43] C. Summonte, R. Rizzoli, M. Bianconi, A. Desalvo, D. Iencinella and F. Giorgis. *J. Appl. Phys.*, 2004, **96**, 3987-3997.

[44] Q. Cheng, S. Xu and K. Ostrikov. *Acta Materialia*, 2010, **58**, 560-569.

[45] D. Das. *Solid State Phenom.*, 1995, **44**, 227.

[46] N.-M. Park, C.-J. Choi, T.-Y. Seong and S.-J. Park. *Phys. Rev. Lett.*, 2001, **86**, 1355-1357.

[47] R. Robertson and A. Gallagher. *J. Chem. Phys.*, 1986, **85**, 3623-3630.

[48] Q. Cheng, S. Xu and K. Ostrikov. *The J. Phys. Chem. C*, 2009, **113**, 14759-14764.

[49] V.L. Dalal, K. Muthukrishnan, X. Niu and D. Stieler. *J. Non-Cryst. Solids*, 2006, **352**, 892-895.

[50] B. E. Vallat-Sauvain, Advances in Microcrystalline Silicon Solar Cell Technologies in Thin Film Solar Cells, in: J.P.a.V. Arkhipov (Ed.) Fabrication, Characterization, and Application, John Wiley and Sons, England, 2007.

[51] S.X. Li, Y.Q. Cao, J. Xu, Y.J. Rui, W. Li and K.J. Chen. *Appl. Surf. Sci.*, 2013, **270**, 287-291.

[52] I.A. Yunaz, K. Hashizume, S. Miyajima, A. Yamada and M. Konagai. *Sol. Energ. Mater. Sol. Cells*, 2009, **93**, 1056-1061.

[53] F. Demichelis, G. Crovini, C.F. Pirri, E. Tresso, G. Amato, U. Coscia, G. Ambrosone and P. Rava. *Thin Solid Films*, 1994, **241**, 274-277.

[54] T. Chen, Y. Huang, D. Yang, R. Carius and F. Finger. *Thin Solid Films*, 2011, **519**, 4523-4526.

[55] S. Miyajima, J. Irikawa, A. Yamada and M. Konagai. *Appl. Phys. Lett.*, 2010, **97**, 023504.

[56] Y. Hattori, D. Kruangam, T. Toyama, H. Okamoto and Y. Hamakawa. *Appl. Surf. Sci.*, 1988, **33–34**, 1276-1284.

[57] Y. Huang, T. Chen, A. Gordijn, A. Dasgupta, F. Finger and R. Carius. *J. Non-Cryst. Solids,* 2008, **354**, 2430-2434.

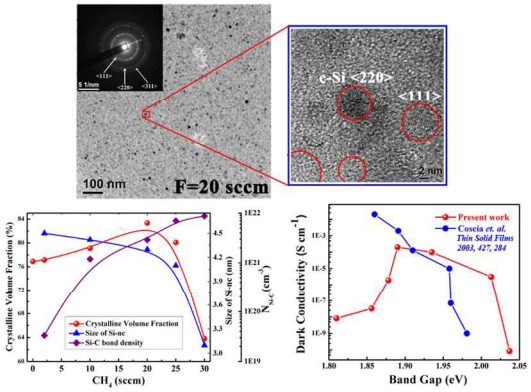

129x50mm (300 x 300 DPI)